The Astrophysical Journal, 571:809–817, 2002 June 1

ROSAT X-RAY OBSERVATIONS OF THE DWARF GALAXY HOLMBERG II

Jürgen Kerp
Radioastronomisches Institut der Universität Bonn, Auf dem Hügel 71, D-53121 Bonn, Germany; jkerp@astro.uni-bonn.de

Fabian Walter
Astronomy Department 105-24, California Institute of Technology, Pasadena, CA 91125; fw@astro.caltech.edu

and

Elias Brinks
Departamento de Astronomía, Universidad de Guanajuato, Apartado Postal 144, Guanajuato, C.P. 36000, Mexico; ebrinks@astro.ugto.mx
Received 2001 October 12; accepted 2002 February 6

ABSTRACT

We present a study of the irregular dwarf galaxy Holmberg II based on *ROSAT* Position Sensitive Proportional Counter observations (total exposure time: 22 ks). Holmberg II is a nearby (3.2 Mpc), well-studied dwarf irregular galaxy. It is famous for its interstellar medium (ISM), which is dominated by expanding structures such as H I holes and shells. We search for X-ray emission from point sources as well as for diffuse emission, down to the detection limit of the *ROSAT* data. Using X-ray hardness ratio diagrams we differentiate between thermal plasma and power-law X-ray spectra, which helps to determine the nature of the individual sources. Correlating the X-ray data with complementary observations ranging from the far-ultraviolet to the radio regime, we increase the probability of correctly identifying sources belonging to Holmberg II. We did not detect soft X-ray emission originating from hot gas within supergiant H I shells above our luminosity sensitivity limit of $L_{\rm limit}(0.1\text{–}2.1\ {\rm keV}) \geq 10^{37}{\rm ergs\ s^{-1}}$. This finding can probably be attributed to blowout in the case of the largest holes and insufficient sensitivity (owing to strong photoelectric absorption) in the case of the smaller H I holes. However, we find faint X-ray sources well beyond the stellar body but within the H I distribution of Holmberg II, which suggests the presence of X-ray binaries. This indicates that star formation has taken place across the entire gaseous disk of Holmberg II in the past, some of which may have created the structures seen in the ISM at large galactocentric radii.

Subject headings: galaxies: dwarf — galaxies: individual (Holmberg II) — galaxies: ISM — X-rays

1. INTRODUCTION

Holmberg II (hereafter Ho II) is one of the most famous examples of a dwarf galaxy exhibiting a violent, disrupted interstellar medium (ISM), as traced by its appearance in the 21 cm H I line (Puche et al. 1992). H I holes are present across the entire galaxy—even well beyond Ho II's stellar body. Puche et al. (1992) compiled a catalog of individual H I shells. The measured radial expansion velocities (10–25 km s^{-1}) and diameters (100–2000 pc) indicate that most of the holes are still expanding and have ages of $t \sim 10^7$–10^8 yr.

Ho II has been studied at many other wavelengths as well, such as radio continuum wavelengths (Tongue & Westpfahl 1995), optical (Rhode et al. 1999), and far-ultraviolet (FUV; Stewart et al. 2000). Besides, it has been the topic of studies to determine its mass distribution and dark matter content (Bureau & Carignan 1997) and a popular galaxy to compare numerical simulations/models of expanding H I shells against (Mashchenko & Silich 1995; Oey & Clarke 1997).

Recent H I observations, including those of Ho II, show that H I holes are older and reach larger sizes in dwarf galaxies, as compared to similar structures in more massive, spiral galaxies. Some of this can be attributed to the fact that dwarf galaxies have shallower gravitational potentials, which leads, for the same observed H I velocity dispersion, to a puffed-up disk. Hence, H I holes can grow to larger sizes before breaking out of the disk. Moreover, dwarf galaxies are lacking in general differential rotation or spiral density waves (e.g., Walter & Brinks 1999). In other words, once formed, structures like H I holes in the ISM are not strongly modified and/or destroyed by large scale streaming motions.

The most straightforward way to interpret the presence of the H I cavities is to attribute them to past stellar activity within their centers (the "standard picture"): strong winds of O and B stars can create individual bubbles of parsec size, whereas subsequent supernova (SN) events create cavities of a few tens to hundreds of parsecs extent. In this picture, the expansion of the H I holes is powered by the overpressure created within the coronal gas resulting from the SN explosions (e.g., Weaver et al. 1977).

Although the standard picture of the creation of the H I holes is widely accepted, it is not without its critics. For example, Rhode et al. (1999), analyzed broadband *BVR* (4 σ detection limit: $B = 23$ mag) and narrowband Hα images to search for star clusters in the centers of the H I holes in Ho II. Based on the results derived by Puche et al. (1992) for the age and energy needed to create the H I hole, and assuming that the stellar cluster remained a coherent structure during its evolution and using conventional initial mass functions, they argue that these star clusters should still be detectable. As their observations revealed far less remnant clusters than expected, Rhode et al. (1999) ruled out clusters as the origin for the H I holes in all but six out of 48 cases. Certainly the giant holes outside the optical disk of Ho II are especially difficult to explain since star formation currently does not seem to play a dominating role at large galactocentric radii of Ho II.

X-ray observations of dwarf galaxies can be used to test the validity of the standard picture. Coronal gas within the interiors of the H I holes might be detectable in X-rays,

whereas objects related to the end points of stellar evolution—such as X-ray binaries—are expected to show up as hard X-ray point sources. Low-mass X-ray binaries are prominent X-ray sources detectable even at the distance of Ho II. In the optical regime, however, these objects are very faint and difficult to detect even with large telescopes. X-ray observations seem the best way forward now to further check the validity of the standard picture.

Zezas, Georgantopoulos, & Ward (1999) as well as Miyaji, Lehmann, & Hasinger (2001) have reported *ROSAT* data on the strongest X-ray source in Ho II only. Here we perform an analysis of all sources related to Ho II within the entire field observed with the *ROSAT* Position Sensitive Proportional Counter (PSPC). Section 2 deals with the data reduction and analysis of three pointed *ROSAT* PSPC observations of Ho II, which we retrieved for that purpose. In § 3 we introduce the X-ray hardness ratio diagram as a tool to classify the X-ray spectrum for faint sources. Our results are presented in § 4, which are then discussed in § 5. We summarize our conclusions in § 6.

2. DATA REDUCTION AND ANALYSIS

2.1. *Archival Data*

We retrieved three pointed PSPC observations toward Ho II from the *ROSAT* archive (see Table 1 for details). The *ROSAT* PSPC data were analyzed using the EXSAS software package, provided by the Max-Planck-Institut für Extraterrestrische Physik in Garching (Zimmermann et al. 1998). All three observations were merged into a single photon event file and recentered on the mean position: $\alpha_{J2000} = 8^h19^m5^s$, $\delta_{J2000} = +70°42'36''$. The net integration time of the merged *ROSAT* PSPC data is 22,566 s, making Ho II one of the deepest studied dwarf galaxies by *ROSAT*. The photon events were binned into the standard *ROSAT* $\frac{1}{4}$ keV (also denoted as *ROSAT* C band), $\frac{3}{4}$ keV (M band), and 1.5 keV (*J* band) energy bands and a total energy band (corresponding to the pulse-height invariant channels 11–41, 52–90, 91–201, and 11–201). We calculated a merged exposure map for each individual X-ray image to overcome the problem of radially decreasing sensitivity and vignetting of the *ROSAT* PSPC.

The radius of the *ROSAT* PSPC point-spread function (PSF) depends on the X-ray photon energy and the off-axis angle with respect to the optical axis, resulting in a varying angular resolution between 23″ and 34″ within an off-axis radius of 10′ from the optical axis. We determined the X-ray background (XRB) intensity level outside the H I distribution of Ho II ($r \geq 10'$), which we subsequently used as the "off" intensity value.

TABLE 1
SEQUENCE NUMBER OF THE *ROSAT* PSPC OBSERVATIONS, THEIR DATE, AND INTEGRATION TIME ON SOURCE

Sequence	Date	t_{int} (s)
600140p	1992 Apr	7258
600431p	1992 Oct	11607
600431p-1	1993 Mar	3701

We integrated the X-ray photons of each individual source within a circular area with a diameter equal to 3.5 times the diameter of the PSF($3.5d_{PSF}$) for each individual energy band. This area covers 99% of the X-ray source photons. From this total number of photons we subtracted the contribution of the XRB, and evaluated the residual X-ray intensity level in the immediate surrounding of the X-ray source. We classified an X-ray source as detected if the number of net counts exceeded the 3 σ threshold above the noise set by the background level.

The results are shown in the left panel of Figure 1, which shows the *ROSAT* PSPC $\frac{1}{4}$ keV map as contours superposed on a gray-scale rendering of the neutral hydrogen distribution (Puche et al. 1992). The right panel shows the X-ray intensity distribution averaged over the entire 0.1–2.1 keV energy range. Figure 2 displays this latter map in the left panel as contours superposed on a 4.86 GHz radio continuum image (Tongue & Westpfahl 1995), whereas the contours in the right panel are overlaid on a map of the Hα emission.

2.2. *Confusion with Cosmic X-Ray Background Sources*

The extragalactic XRB is due to the superposed emission of individual objects, mostly active galactic nuclei and quasi-stellar objects (Hasinger et al. 1998; Mushotzky et al. 2000). Unfortunately, the angular resolution of the *ROSAT* PSPC does not allow one to resolve faint individual XRB sources; i.e., the PSPC is confusion limited. To constrain the contribution of the diffuse extragalactic XRB radiation, one has to evaluate the overall spectral characteristics of this X-ray emission component. Gendreau et al. (1996) showed that the extragalactic XRB emission can be approximated by a power law with $I(E) \propto E^{-\Gamma}$ and $\Gamma \simeq 1.5$. They determined an intensity of the extragalactic XRB at 1 keV of about 9.6 keV cm^{-2} s^{-1} sr^{-1} keV^{-1}.

Taking this value for the XRB and assuming that the extragalactic XRB is only attenuated by the ISM of the Milky Way, we derive within the area of an individual X-ray source toward Ho II ($3.5d_{PSF}$) an X-ray flux for the extragalactic XRB of about $F_{XRB} = 2.8 \times 10^{-15}$ergs cm^{-2} s^{-1}.

So far, we have been focusing on the overall extragalactic XRB flux level. However, we must take into account the $\log N$ versus $\log S$ relation (Hasinger et al. 1998) to evaluate the frequency of extragalactic XRB sources at a certain flux level. Unfortunately, there is no straightforward way to discriminate between unrelated background sources and those belonging to Ho II. However, we can reduce this ambiguity by studying the X-ray colors of a source and by searching for counterparts at other wavelengths using complementary data (which is what we will do in the following). Extragalactic sources unrelated to Ho II—and absorbed by its gas distribution—will appear as hard X-ray sources, detectable preferentially in the *ROSAT* M and *J* bands. The 3 σ X-ray flux level across the entire *ROSAT* energy band is $F_{3\sigma}(0.1\text{–}2.1 \text{ keV}) = (4.1 \pm 1.4) \times 10^{-15}$ ergs cm^{-2} s^{-1}, above the diffuse extragalactic background level. Applying the $\log N$ versus $\log S$ relation derived by Hasinger et al. (1998) to the area of Ho II H I gas distribution, we expect to detect about seven significant X-ray sources unrelated to Ho II.

Assuming a distance to this object of 3.2 Mpc and a galactic X-ray–attenuating column density of $N_{HI} = \sim 3 \times 10^{20}$ cm^{-2} (Hartmann & Burton 1997), we derive a detection

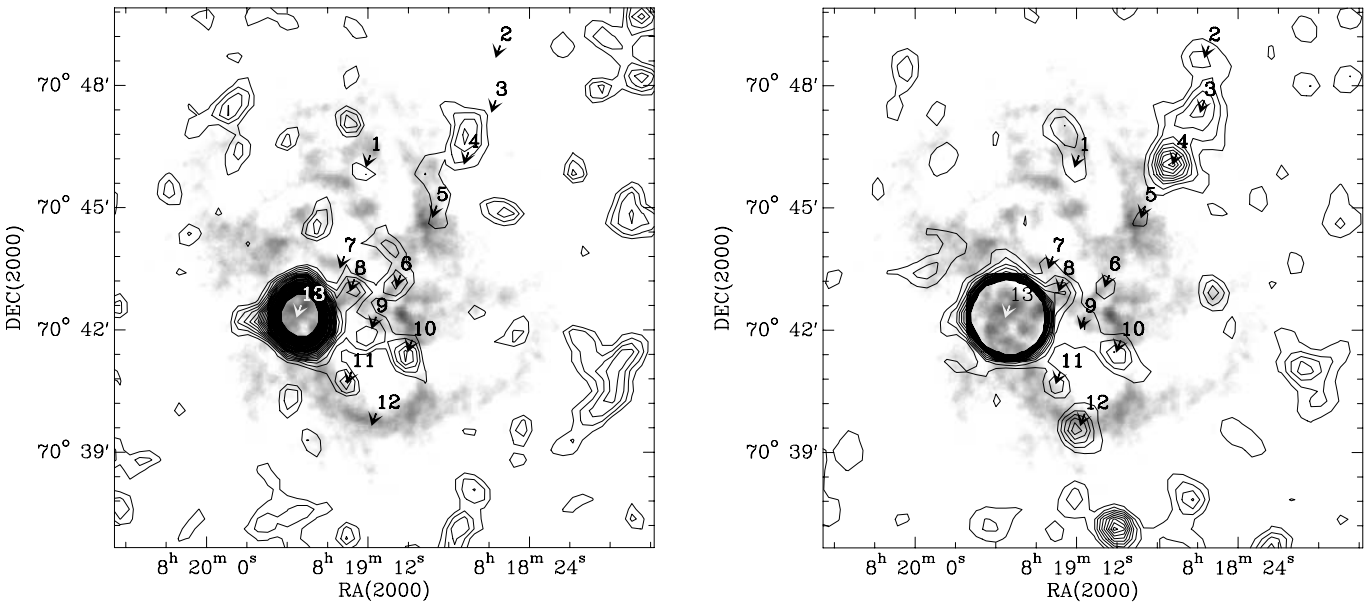

FIG. 1.—*Left*: *ROSAT* PSPC $\frac{1}{4}$ keV intensity distribution superposed as contours on the H I 21 cm map of Ho II. The numbers denote the X-ray sources according to Table 2. The arrows point to the center of each X-ray source. The contour lines start at the 3 σ level, in incremental steps of 1 σ (angular resolution smoothed to 75″). *Right*: *ROSAT* PSPC total (0.1 keV to 2.1 keV) X-ray intensity distribution superposed as contours on the H I 21 cm map of Ho II. The contour lines start at the 3 σ level incrementing in steps of 2 σ. Note that the individual sources 2, 3, 4, and 12 are not positionally coincident with $\frac{1}{4}$ keV X-ray sources and thus may be unrelated background sources (see discussion in the text).

luminosity threshold of $L_{3\sigma} \geq (10.8 \pm 3.6) \times 10^{36}$ ergs s^{-1} for sources associated with Ho II (neglecting for the moment absorption within this galaxy). Only very young supernova remnants or accreting X-ray binaries typically exceed this threshold. The *ROSAT* PSPC X-ray data presented here therefore trace only two extreme populations in Ho II: the actual population ($t < 10^5$ yr; i.e., supernova remnants) or a population older than $t > 10^7$ yr, such as pulsars or accreting X-ray binaries. The intermediate age stellar population can be traced via Hα and FUV observations (Stewart et al. 2000). Combining all data provides a unique picture of the star formation history of Ho II over the last 100 Myr.

3. THE HARDNESS RATIO DIAGRAM

In this section we introduce a useful tool to constrain the spectral properties of faint X-ray sources. Using this tool it becomes possible to estimate whether the spectrum of a (faint) X-ray source is predominantly characterized by a

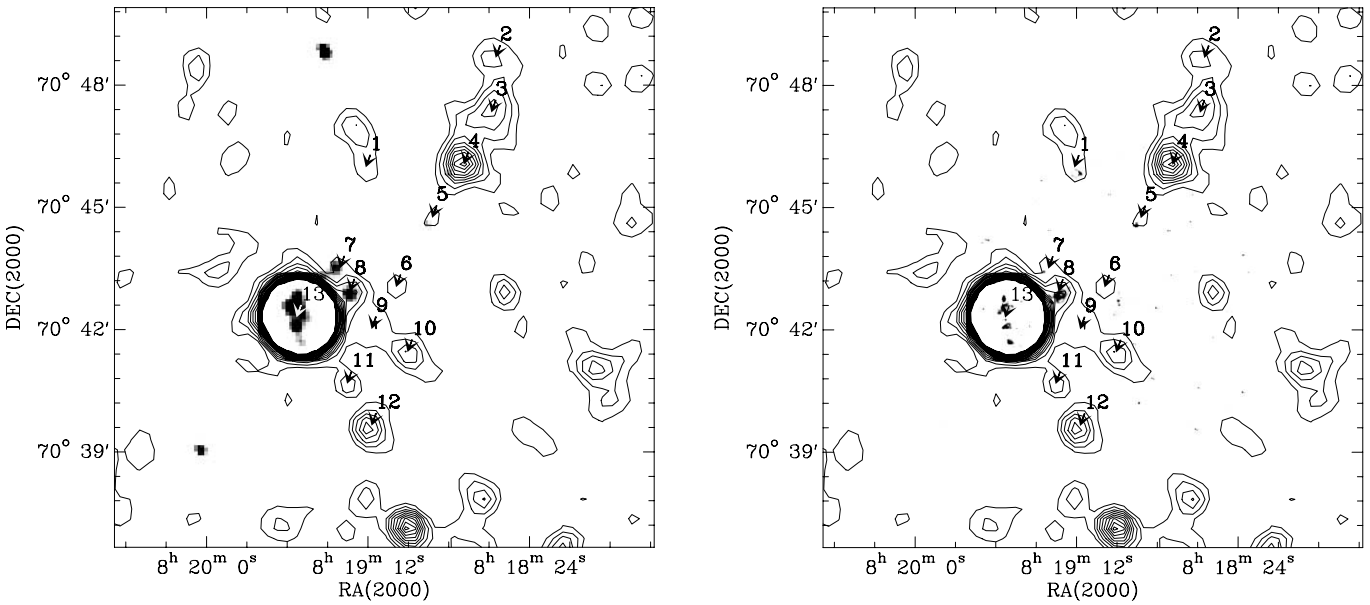

FIG. 2.—*Left*: Superposed on a gray-scale representation of the 4.86 GHz radio continuum Very Large Array map of Ho II are the contour lines of the total (0.1–2.1 keV) X-ray intensity distribution. The contours start at 3 σ incrementing in steps of 2 σ (angular resolution smoothed to 75″). *Right*: Hα map of Ho II superposed by the contour lines corresponding to the total *ROSAT* energy window, as presented from the left. The available Hα map only covers parts of the region of interest.

thermal emission spectrum or rather by a power law. We first briefly discuss the characteristics of those sources likely to be encountered in our object and then proceed to explain what we call the hardness ratio diagram and where these different sources are likely to be encountered in these diagnostic diagrams.

Supernova remnants are characterized by their thermal plasma radiation. Below a temperature of $T \simeq 10^{6.4}$ K, emission lines dominate the X-ray spectrum. Above this temperature, Bremsstrahlung is the most important cooling mechanism of the hot plasma. The cooling time of the plasma can be approximated via $t_{\rm cool} \simeq (3/2)(NkT/\Lambda_N n_t n_e) \propto [(T)^{1/2}/n_e]$, where N is the total number of particles, T is the hot plasma temperature in kelvins, n_t the ion density, n_e the electron density (both in cm^{-3}), and Λ_N the normalized cooling rate (Sutherland & Dopita 1993). This leads to $t_{\rm cool} \simeq 10^9$ yr, assuming a temperature of $T \simeq 10^{6.4}$ K and a typical electron density of about $n_e = 2 \times 10^{-3}$ cm^{-3}. The expected X-ray luminosity of a single young SN is $L_{\rm X} \sim 10^{38}$ ergs s^{-1} (Fabbiano 1996).

Core-collapse supernovae are correlated in space and time, their progenitor having been formed in groups, OB associations, or even larger conglomerates. Expanding individual supernova remnants are therefore likely to merge, creating expanding shells referred to in the literature as superbubbles or supergiant shells, which are supposedly filled with tenuous, high-temperature gas. These shells show up in H I maps as holes in the neutral hydrogen distribution. In the case of Ho II, the largest holes have diameters roughly twice the 1 σ scale height of the H I disk of 600 pc, according to Puche et al. (1992). The cooling time of the coronal gas within the interior of the shells is much longer than the ages of the H I holes, which should make them detectable in X-rays. However, the largest supershells, with diameters exceeding 1 kpc, likely broke out of the disk, at which moment the hot gas interior is vented in to the halo, the hot plasma is lost, and the hole becomes invisible in X-rays. In the case of the smaller, still confined holes, the interior X-ray emission should be detectable if the H I column density of the approaching side of the H I shell does not exceed values of $N_{\rm H\,I} \geq 5 \times 10^{20}$ cm^{-2}, above which value the soft X-ray emission ($E \leq 0.5$ keV) of the hot gas is absorbed in situ by the shell.

Pulsars, cooling neutron stars, as well as accreting X-ray binaries are the very end points of stellar evolution and may be observable within the interior of the holes, under the assumption that the origin of the holes is caused by star-forming activity and subsequent rapid stellar evolution of the most massive stars. Their X-ray luminosities typically range between $L_{\rm X}(0.1\text{–}2.4\ {\rm keV}) \simeq 10^{36}$ and 10^{38} ergs s^{-1}.

To identify the emission mechanism of an X-ray source the standard procedure is to extract a spectrum from the X-ray data. The brightest source associated with Ho II has previously been studied in this way by Zezas et al. (1999). However, owing to the large number of free parameters, even the analysis of this high signal-to-noise X-ray spectrum is not without its ambiguities.

In the case of faint X-ray sources [$F_{\rm X} \simeq (5\text{–}20) \times 10^{-15}$ ergs cm^{-2} s^{-1}], which are discussed here, the insufficient signal-to-noise ratio does not allow us to extract much information from the *ROSAT* PSPC spectra. However, the count rates within the individual broad *ROSAT* energy bands contain significant information about the X-ray source spectrum. We therefore decided to study the hardness ratios to constrain the X-ray emission process. For this aim, we subtracted the contribution of the extragalactic X-ray background emission from the count rates of the individual X-ray sources. In Figure 3 we plot the *ROSAT* hardness ratio 1 (HR1) [$(M + J - C/C + M + J)$] versus the *ROSAT* hardness ratio 2 (HR2) ($J - M/M + J$). The stronger the photoelectric absorption, the harder the resulting X-ray spectrum. The lines in the figure indicate the locus where one can expect individual sources to fall in the hardness ratio diagram, depending on the type of X-ray emission, either thermal or power law, over a range of temperatures and power-law indices, respectively, and over a range of foreground absorptions. This latter effect is quite comparable to the reddening caused by intervening dust in an optical color-color diagram.

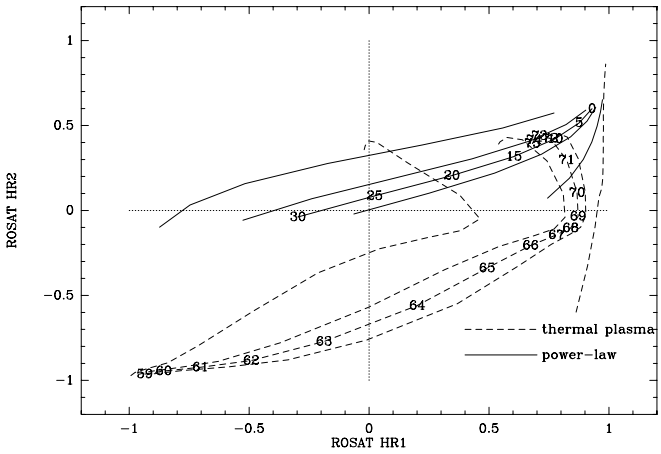

FIG. 3.—Hardness ratio diagram. Solid lines represent the expected hardness ratio locus for power-law X-ray spectra; dashed lines mark thermal plasma spectra. The tracks have as a free parameter the X-ray–absorbing column density. Starting leftmost with the unabsorbed situation, $N_{\rm H\,I} = 0$, 2, 3, and 4×10^{20} cm^{-2}. The numbers along the $N_{\rm H\,I} = 3 \times 10^{20}$ cm^{-2} track give the energy index in case of power law and log T(K) in the case of thermal plasma spectra. To illustrate the case of very high column densities, we also plotted the color-color tracks for $N_{\rm H\,I} = 10 \times 10^{20}$ cm^{-2}, both for thermal plasma emission and for power-law X-ray spectra.

The relations displayed in Figure 3, for both the power law (*solid lines*) as well as the thermal plasma spectra (*dashed lines*)—assuming solar metal abundances—are plotted for increasing absorbing foreground column density (from left to right, $N_{\rm H\,I} = 0$, 2, 3, and 4×10^{20} cm^{-2}). The leftmost relation of both the power law or the thermal case represents the unabsorbed situation. The numbers along the tracks for $N_{\rm H\,I} = 3 \times 10^{20}$ cm^{-2} (which corresponds to the absorbing foreground column density corresponding to the Milky Way; Hartmann & Burton 1997) give the spectral slope for the power-law spectra (*solid lines*) and log T(K) in case of the thermal plasma spectra. Obviously, soft X-ray sources will predominantly be found in the lower left part of the X-ray hardness ratio diagram, whereas highly absorbed or intrinsically hard X-ray sources populate the upper right part of the diagram.

4. RESULTS

In total, we detected 31 significant X-ray sources within the extent of the H I distribution of Ho II. As mentioned earlier, only seven X-ray sources are expected, based on the log N versus log S relation derived by Hasinger et al. (1998).

TABLE 2

COMPILATION OF *ROSAT* X-RAY SOURCES THAT COINCIDE IN POSITION WITH COUNTERPARTS AT OTHER WAVELENGTHS

Number	α_{J2000}	δ_{J2000}	F_X ($\times 10^{-15}$ ergs cm^{-2} s^{-1})	L_X ($\times 10^{37}$ ergs s^{-1})	Source Detection[a]	C-Band Source
1.....	08 19 12	70 45 59	11.1 ± 2.2	2.4 ± 0.6	FUV	x
2.....	08 18 34	70 48 40	14.7 ± 2.6	3.3 ± 0.6	RCS/thermal X-ray	...
3.....	08 18 35	70 47 20	34.6 ± 4.0	7.7 ± 0.9	...	...
4.....	08 18 43	70 46 03	45.4 ± 4.5	10.1 ± 1.0	FUV, RCS, X-ray thermal, or power law	...
5.....	08 18 53	70 44 45	4.8 ± 1.5	1.1 ± 0.3	FUV, thermal RCS, Hα	x
6.....	08 19 03	70 43 03	4.8 ± 1.5	1.1 ± 0.3	FUV, thermal RCS, Hα	x
7.....	08 19 20	70 43 30	42.8 ± 4.4	9.5 ± 1.0	FUV, SNR RCS, X-ray power law, Hα	x
8.....	08 19 17	70 42 56	140.4 ± 7.9	31.5 ± 1.8	FUV, thermal RCS, X-ray thermal, Hα	x
9.....	08 19 11	70 42 01	20.1 ± 3.0	4.4 ± 0.7	FUV, Hα	x
10.....	08 19 00	70 41 27	16.5 ± 2.7	3.6 ± 0.7	FUV, Hα	x
11.....	08 19 18	70 40 40	20.2 ± 2.1	2.2 ± 0.4	FUV	x
12.....	08 19 10	70 39 39	22.8 ± 3.2	5.1 ± 0.7	FUV, RCS, X-ray thermal, or power law	...
13.....	08 19 33	70 42 18	3981.2 ± 42.1	882.1 ± 9.4	FUV, SNR RCS, X-ray thermal, Hα	x

NOTE.—Units of right ascension are hours, minutes, and seconds, and units of declination are degrees, arcminutes, and arcseconds.

[a] The most likely origin for the X-ray flux, as well as information from the complementary data; "RCS" denotes radio continuum source. The radio data is published by Tongue & Westpfahl 1995, the optical data by Rhode et al. 1999, and the FUV data by Stewart et al. 2000.

[b] The "x" indicates if a source emits significant amounts of $\frac{1}{4}$ keV radiation, suggesting that the X-ray source is located in front of the gaseous body of Ho II.

To avoid any confusion with unrelated extragalactic XRB sources, we decided to study only those X-ray sources that are identified in at least one additional frequency range. This complementary information also gives us a better handle on the nature of the X-ray source in question. This left us with 13 sources, all believed to be related to Ho II. The properties of these 13 sources (positions, fluxes, luminosities, complementary data) are listed in Table 2. We mark with an "x" those sources that emit significant soft ($\frac{1}{4}$ keV) X-ray photons, implying that they are most likely associated with Ho II. Because a background X-ray source will be attenuated by the entire amount of ISM belonging to Ho II, this leads to strong photoelectric absorption, reducing especially the soft part of the X-ray spectrum. We tried to constrain the X-ray emission process further by studying the spectral properties of the X-ray sources via the hardness ratio diagram (§ 3).

4.1. *X-Ray Sources inside* H I *Holes*

The *ROSAT* $\frac{1}{4}$ keV map (Fig. 1) shows the emission that is most likely associated with X-ray plasma radiation. Because of the fairly high luminosity limit of the *ROSAT* observations [$L_{\rm limit}(0.1\text{–}2.1\ {\rm keV}) \geq 10^{37}$ergs s^{-1}], supernova remnants are the most likely candidates to be encountered.

The X-ray sources 6, 7, 9, 10, and 13 are associated with H I holes cataloged by Puche et al. (1992); their centers are located within the extent of the H I holes (for details, see Table 2). Although these soft X-ray sources are located within the low volume density cavities of Ho II, one cannot exclude a chance association with an extragalactic X-ray background source. The X-ray sources that most probably belong to Ho II should be detectable simultaneously in the radio and/or the optical regime. Sources 7, 8, and 13 are positionally coincident with radio continuum emission (see Fig. 2, *left*; also Tongue & Westpfahl 1995).

According to Tongue & Westpfahl (1995), X-ray source 7 (H I hole 36) coincides with a steep spectrum nonthermal radio source. In Figure 4 we plot all X-ray sources brighter than 11×10^{-15} ergs cm^{-2} s^{-1} in a hardness ratio diagram similar to the one presented in Figure 3. This suggests for source 7 a steep X-ray energy power-law spectrum [$I(E) \propto E^{-2.5}$], implying an accreting X-ray binary system as a likely source of the radiation (White, Swank, & Holt 1983). Tongue & Westpfahl (1995) favor an extragalactic origin, unrelated to Ho II, because they interpret the steep radio continuum spectrum as an indication for spectral aging of the electron population which is frequently discussed in the framework of evolutionary models of radio galaxies. However, the X-ray as well as the positionally coincident radio continuum source fits very well within the H I hole 36 of the Puche et al. (1992) catalog. Moreover, close to X-ray source 7 a small H II region is located (Fig. 2). One may speculate that this H II region and associated Hα emission is due to secondary star formation, on the rim of H I hole 36 (Puche et al. 1992).

The X-ray sources 6, 9, and 10 are not exactly coincident with Hα or radio continuum emission. However, Hα and radio continuum radiation is present within the $3.5d_{\rm PSF}$ diameter discussed earlier, which is why we included these sources in our analysis. Close to the southern boundary of

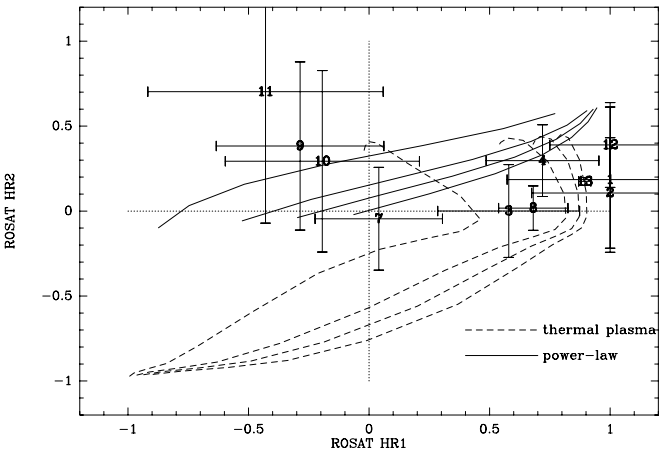

FIG. 4.—Same as Fig. 3, but the X-ray sources brighter than $F_X \times 10^{-14}$ ergs cm^{-2} s^{-1} are labeled according to the numbers given in Table 2.

source 6 (H I holes 22 and 23), Hα and thermal radio continuum emission indicate the presence of a patchy star-forming region. The FUV data of Stewart et al. (2000) suggest a young star-forming region with an age of 2.5–3.5 Myr. Inspection of Table 2 of Rhode et al. (1999) supports the view that X-ray source 6 (positionally coincident with H I hole 22) is associated with a stellar cluster.

The X-ray sources 9 (H I hole 29 and 32) and 10 (H I hole 21) are associated with faint Hα and FUV emission at their rims. The FUV data imply an age of greater than 6.3 Myr (Stewart et al. 2000). This is consistent with the findings based on the X-ray hardness ratio diagram (Fig. 4) and suggests power-law spectra for both X-ray–emitting sources. Their X-ray luminosities of a few 10^{37} ergs s^{-1} classify both as likely candidates of accreting binary systems (White et al. 1983).

4.2. *X-Ray Sources outside* H I *Holes*

Sources 1, 5, 8, and 11 are located outside H I holes, toward high column density regions of Ho II. The accidental association with an extragalactic XRB source becomes much less likely, because of the strong attenuation of a possible unrelated extragalactic soft X-ray source by the significant amounts of X-ray–absorbing matter within Ho II (in addition to the roughly constant absorption owing to the Milky Way).

Source 1 is associated with bright Hα and FUV emission; however, it is not detected in radio continuum maps. This can be interpreted as an indication for a developed star cluster with evolved stars, which already partly left the main sequence.

The FUV data implies an age of greater than 6.3 Myr. The X-ray emission is too faint to set constraints on the most likely X-ray emission process, even when employing the hardness ratio diagram. So no firm conclusions as to the nature of the source can be derived from the available data.

Source 5, which shows X-ray emission at the 3 σ level, coincides with a radio continuum source. Tongue & Westpfahl (1995) derived a thermal radio continuum spectrum for that source from their multifrequency analysis. This is consistent with the Hα map (Fig. 2, *right*), which shows a compact H II region at this position. Therefore, the most likely conclusion regarding the nature of this source is that of a young star-forming region.

Source 8 emits thermal radio continuum emission as well. This is consistent with the Hα map of Ho II (Fig. 2), which reveals a very prominent H II region at this location. The linear extent of the H II region is on the order of 100 pc. The X-ray hardness ratio diagram also implies a thermal origin of the detected X-ray emission [$\log T(\mathrm{K}) \simeq 7$]. A single luminous O star has a luminosity of about $L_{\mathrm{X}}(\mathrm{O\ star}) \simeq 10^{34}$ ergs s^{-1} in the *ROSAT* X-ray energy window (Kudritzki et al. 1995). Therefore, we would require a contribution by several hundred young stars in order to account for the observed X-ray emission. Because the radio continuum spectrum is thermal in nature, the region has to be very young as otherwise supernovae and their remnants would start to dominate the radio continuum spectrum with a nonthermal component.

Taking into consideration that the Hα ridge related to source 8 is located between the boundaries of two H I holes (holes 29 and 36), very recent induced star formation may be taking place here. Stewart et al. (2000) derived an age of 3.5–4.5 Myr for that particular region, consistent with the presence of a young massive star-forming region. Additional evidence for a stellar cluster is provided by the optical search for stellar emission within the H I holes performed by Rhode et al. (1999), who report that a stellar cluster may underlie the nearby H I hole 36.

X-ray source 11 is of interest because the analysis of Stewart et al. (2000) implies a young star-forming region, with an age of 2.5–3.5 Myr, whereas this region is not detected in the Hα map. Its location in the X-ray hardness ratio diagram implies a power-law X-ray spectrum, indicating an accreting compact object. Both the absence of Hα radiation and the X-ray data suggest that toward this high column density region we observe more likely the end point of stellar evolution, like an X-ray binary.

4.3. *X-Ray Sources outside the Stellar Disk*

Sources 2, 3, 4, and 12 are located far beyond the stellar distribution. Sources 2 and 4 are associated with faint radio continuum emission. Both sources are prominent within the *ROSAT* $\frac{3}{4}$ keV and the 1.5 keV energy band, whereas in the $\frac{1}{4}$ keV map they are only seen at the 3 σ level. This indicates that both sources have a hard intrinsic X-ray spectrum or, alternatively, are highly absorbed X-ray sources. The hardness ratio diagram implies, in the case of source 2, that its emission may be associated with thermal plasma radiation. In the case of source 4, it is not possible to differentiate between a power law and a thermal plasma X-ray spectrum.

Source 3 is located in between both sources. These three sources appear in the X-ray map as a coherent structure. Source 3 is visible at high signal-to-noise level in the *ROSAT* $\frac{1}{4}$ keV map (Fig. 1). Together with the fact that it is situated toward high H I column densities suggests that this source is associated with Ho II and not located beyond its $N_{\mathrm{H\,I}}$ column density distribution. This is why we decided to include this source in Table 2. However, the complementary data do not reveal any obvious counterpart for source 3.

Finally, source 12 is located toward a high H I column density region of Ho II. Neither in the radio continuum nor in the Hα map (Fig. 2) is there any emission associated with this particular source. The FUV map of Stewart et al. (2000), however, revealed excess emission positionally coincident with this particular source. Quite comparable to the case of source 11 (see discussion above), the analysis of Stewart et al. (2000) argues for a young star-forming region of 2.5–3.5 Myr, whereas the X-ray data does not exclude the possibility that an end point of stellar evolution may account for the observed X-ray emission. This hypothesis is furthermore supported by the absence of Hα emission. The X-ray luminosity of source 12, with $L_{12} = (2.28 \pm 0.32) \times 10^{38}$ ergs s^{-1}, is compatible with both a supernova remnant or an accreting binary system.

4.4. *The Brightest X-Ray Source in Ho II*

The brightest X-ray source, labeled source 13 in this paper, has been the subject of papers by Zezas et al. (1999) and Miyaji et al. (2001). This source dominates the entire X-ray emission of Ho II, because 87% of all detected photons emerge from this unique object. Without its contribution the total X-ray luminosity of Ho II would only be about $L_X \simeq 1 \times 10^{39}$ ergs, which is equivalent to the added X-ray luminosities of about six high-mass X-ray binaries. In this respect, Ho II is not a spectacular object in X-rays. Here we

reanalyze this object using the X-ray hardness ratio diagram. This source can be very well approximated by a single-component thermal X-ray spectrum with a temperature of $\log T(\mathrm{K}) = 7.0$ and an absorbing column density of $N_{\mathrm{H\,I}} = 4 \times 10^{20}$ cm^{-2} Fig. 3, *dashed line on far right*). The neutral hydrogen column density of $N_{\mathrm{H\,I}} = 3 \times 10^{20}$ cm^{-2} [*dashed line with the* $\log T(\mathrm{K})$ *values*] does not fit the hardness ratios of source 13 within the uncertainties. This implies that source 13 is located within a low-density cavity within the ISM of Ho II, as at least 3×10^{20} cm^{-2} is due to Galactic foreground extinction, leaving at most $N_{\mathrm{H\,I}} = 1 \times 10^{20}$ cm^{-2} to any residual column density of gas belonging to the gaseous body of Ho II along the line of sight to source 13. Comparing the plasma temperature based on the X-ray hardness ratio diagram with the results of Zezas et al. (1999), our temperature value falls in between the extreme temperatures derived by them. The X-ray–attenuating column density implied by the X-ray hardness ratio diagram, however, is significantly lower than that derived by these authors.

If one wanted to explain the hardness ratios of source 13 with a power-law spectrum, one would have to assume that the X-ray spectrum of this source is highly absorbed (see Fig. 3). None of the four plotted tracks representing the power-law X-ray spectra fit the position of source 13 in the hardness ratio diagram. Inspecting Table 2 of Zezas et al. (1999) shows that a power-law X-ray spectrum would require an absorbing column density of about $N_{\mathrm{H\,I}} = 1.2 \times 10^{21}$ cm^{-2}, implying that according to the $N_{\mathrm{H\,I}}$ of Puche et al. (1992), source 13 would have to be located on the far side of Ho II or deeply embedded within a molecular cloud.

To constrain the nature of source 13 further, we consider the X-ray luminosities of likely X-ray–emitting candidates. Accreting binaries have typical luminosities of $L_{\mathrm{X}} \simeq 10^{36}$–$10^{38}$ ergs s^{-1}. Source 13, however, has $L_{\mathrm{X}} \geq 10^{40}$ergs s^{-1}. On the other hand, several supernova events are observed with reported X-ray luminosities of $L_{\mathrm{X}} \geq 10^{40}$ ergs s^{-1} (Fabbiano 1989; Fabian & Terlevich 1996). The supernova hypothesis appears to be a more likely explanation than a highly unusual X-ray binary system, which exceeds the Eddington limit. The supernova hypothesis is further supported by the radio continuum data (Tongue & Westpfahl 1995). They classified a positionally coincident radio continuum source as a supernova remnant.

Partial support for this interpretation comes from Miyaji et al. (2001), who applied a wobble correction to the *ROSAT* HRI image of Ho II and claim that 25% of the emission from this source is due to an extended component with a diameter on the order of 10″. Their *ASCA* data reveal, in addition to confirming a soft component which they attribute to (multiple) supernovae, a power-law component accounting for most of the flux density beyond 2.5 keV, implying the presence of an intermediate-mass black hole. A more definitive description of the nature of source 13 will have to await *Chandra* or *XMM-Newton*.

5. DISCUSSION

5.1. *Unresolved Sources*

A casual inspection of Figure 4 shows that most of the X-ray sources of interest lie above the track with $N_{\mathrm{H\,I}} = 3 \times 10^{20}$ cm^{-2}, which is in excellent agreement with what is expected from foreground extinction owing to the Milky Way (Hartmann & Burton 1997). This is an important result as it implies that the X-ray sources are not deeply embedded within the ISM of Ho II.

Of the five X-ray sources located within the interiors of H I holes cataloged by Puche et al. (1992), two of them appear to be associated with supernova remnants (sources 7 and 13), one can be identified with a young star-forming region (source 6), and the remaining two are most likely associated with the end points of stellar evolution, more specifically, accreting X-ray binaries (sources 9 and 10).

Four X-ray sources are located toward high column density regions of Ho II. Because of their location in the soft part of the X-ray hardness ratio diagram, and given that they would have been fully absorbed if they were located beyond the high column density regions, they must be in front of most of the H I, and hence it is likely that they are sources related to Ho II. One may be associated with an evolved stellar cluster (source 1), two with young star-forming regions (sources 5 and 8) and one with an accreting X-ray binary system (source 11).

We find four X-ray sources that are located far beyond the stellar body and close to the edges of the H I column density distribution of Ho II. All sources are either supernova remnants or X-ray binaries. The importance here is that even though there is no evidence based on optical imaging (Rhode et al. 1999) of past star formation, this implies that star formation has occurred some 10^8 yr ago at large galactocentric radii. This suggests that in general the supergiant H I holes may indeed be residuals from energetic events associated with past star-forming activity of Ho II, on timescales $t > 10^9$ yr.

As most sources are too weak to derive an X-ray spectrum, we developed a classification based solely on the hardness ratio diagram. The faintest source analyzed in this way has an X-ray flux of only $F_{\mathrm{X}}(0.1\text{–}2.4\ \mathrm{keV}) = 11 \times 10^{-15}$ ergs cm^{-2} s^{-1}. Although not conclusive, the hardness ratio diagram allows a separation between sources with thermal and power-law spectra.

To reach a firmer conclusion as to the nature of the X-ray sources we combined all available information ranging from the X-ray to the low-frequency radio regime. All but one of the X-ray sources, source 2, are associated with FUV emission, as presented by Stewart et al. (2000), confirming their spatial correlation with regions of recent, massive star formation.

Some of the X-ray emission of Ho II is associated with H II regions. This correlation remains somewhat tentative, however, as we have to take into account that the X-ray detection threshold is high, strongly selecting only the brightest star-forming regions. More sensitive *Chandra* and *XMM-Newton* observations will overcome this instrumental limitation. In the case of X-ray source 8, the Hα, radio continuum, and X-ray data indicate independently the presence of a massive star-forming region. Because of its location in between two prominent H I holes, we speculate that one of the holes might be reheated by a recent supernova event (X-ray source 7); one may then further speculate that this is evidence for induced star formation.

5.2. *Extended Emission*

The *ROSAT* observations reported here did not reveal any hot gas associated with the H I holes. At first sight this

might seem remarkable. For example, in the Milky Way, several hot-plasma filled H I cavities are known. The most prominent one is the local bubble that encloses the Sun (Sfeir et al. 1999). Its X-ray emission is very soft [$\log T(\mathrm{K}) \leq 6.0$] and faint. However, its pressure of $P_{\mathrm{local}} \simeq 10^4$ K cm^{-3} is a factor of 2–5 higher than that of the neutral clouds located within the cavity. Hence, this local cavity presumably is a low-volume density region produced by several supernova events, the latest supernova event dating back to $(1\text{–}2) \times 10^6$ yr. Another interesting Galactic feature is the X-ray–bright supershell known as Loop I, or the North Polar Spur (Egger & Aschenbach 1995). Loop I has a diameter of about ~300 pc. Its temperature is $\log T_{\mathrm{Loop\,I}}(\mathrm{K}) = 6.7$, much higher than that of the local X-ray plasma. It is highly overpressured ($P_{\mathrm{Loop\,I}} = 2.5 \times 10^4$ K cm^{-3}) and still expanding.

Observed with *ROSAT* from a hypothetical vantage point, such as an external galaxy, both X-ray features would have remained undetected because the photoelectric absorption of the enclosing thin neutral shell with $N_{\mathrm{H\,I}} \sim 3 \times 10^{20}$ cm^{-2} is sufficiently high for the X-ray photons originating within the interior of the shell to be absorbed. The only extragalactic detections of hot gas in superbubbles claimed thus far are restricted to dwarf galaxies. Examples are the supergiant shell LMC 4 (Bomans, Dennerl, & Kürster 1994) and the superbubbles N44 and N11 (Chu et al. 1993; Mac Low et al. 1998), all three situated in the LMC. Other examples are the supergiant shell SGS 2 in NGC 4449 (Bomans, Chu, & Hopp 1997) and the possible supershell near Holmberg IX (Miller 1995).

Recently, Walter et al. (1998) detected marginally extended X-ray emission coinciding with a supergiant shell in IC 2574 in a pointed *ROSAT* observation. They found an X-ray luminosity ($D = 3.2$ Mpc) of $(1.6 \pm 0.5) \times 10^{38}$ ergs s^{-1}. Assuming, as usual, a Raymond-Smith model (Raymond & Smith 1977), they derived a plasma temperature of $\log T(\mathrm{K}) = 6.8 \pm 0.3$ and an internal density of $n_e = (0.03 \pm 0.01)$ cm^{-3}. The internal pressure of $P \approx 4 \times 10^5$ K cm^{-3} is again much higher than the pressure of the ambient warm neutral and ionized medium ($P \approx 10^3$–10^4 K cm^{-3}), which led them to suggest that it is probably this hot gas that is still driving the expansion of the shell (see, e.g., Weaver et al. 1977). However, follow-up observations with *Chandra* indicate that the *ROSAT* source is more compact.

In short, only a few, possibly pathological holes, are detected in X-rays. We should not be too surprised, as several authors have pointed out that the X-ray luminosity of the thermal gas expected to fill the superbubbles is well below the *ROSAT* detection limit (Chu & Mac Low 1990; Chu et al. 1995; Mac Low et al. 1998; Silich et al. 2001) The expected X-ray luminosity can be written according to Martin & Kennicutt (1995, their eq. [6]; see also Silich et al. 2001):

$$L_{\mathrm{X}} = 2.12 \times 10^{36}\, L_{38}^{33/35} n_0^{17/35} t_6^{19/35} \kappa_0^{4/7}\ \mathrm{ergs\ s^{-1}}, \quad (1)$$
$$\simeq 2 \times 10^{36} L_{38} \sqrt{n_0 t_6 \kappa_0}\ \mathrm{ergs\ s^{-1}},$$

where L_{38} is the mechanical energy expressed in units of 10^{38} ergs s^{-1}, n_0 the ambient density in atoms cm^{-3}, t_6 the age of the superbubble in Myr and κ_0 a dimensionless scaling factor for the classical conductivity (≤ 1). The metalicity ($Z/Z_\odot$) also influences the luminosity in the X-ray domain. According to Sutherland & Dopita (1993), the dependence of L_{X} on Z can be approximated by $L_{\mathrm{X}} \propto Z^{1/3}$. For example, in a low-metalicity ISM with $Z = 0.1\ Z_\odot$, the expected X-ray luminosity of an X-ray plasma will only be reduced by a factor of 3, not by an order of magnitude. In the case of Ho II (metallicity: about 0.25 $Z_\odot$; Hunter & Gallagher 1985), the expected X-ray luminosity will only be marginally reduced. The "standard supernova" described by equation (1) will expand into an ambient neutral medium, with a typical density ranging between $0.1 \leq n_0 \leq 100$. The age of an expanding structure can be estimated from H I (Puche et al. 1992) and FUV data (Stewart et al. 2000) to a few tens of 10^6 yr. Taking Puche et al. (1992) values of the total mechanical energy needed to create the holes of $E \geq 10^{51}$ ergs, we can calculate the range of expected X-ray luminosity from equation (1). Assuming a conductivity of at least $\kappa_0 = 0.5$ gives a range of $2 \leq (n_0 t_6 \kappa_0)^{1/2} \leq 50$. According to (Puche et al. 1992) and (Stewart et al. 2000) the mechanical energy ranges between $0.03 \leq L_{38} \leq 0.3$. This leads to predicted values of $L_{\mathrm{X}} \approx 10^{36}$–$10^{37}$ ergs s^{-1}. A supernova remnant evolving within a high volume density environment has the highest probability to be detected in X-rays with *ROSAT*. As an example, source 7 and H I hole 36 are positional coincident; using $t_6 = 10$ (Stewart et al. 2000) and $E = 86 \times 10^{50}$ ergs (Puche et al. 1992) gives $L_{38} = 0.27$. With $n_0 = 100$ cm^{-3} and $\kappa_0 = 0.5$ we derive $L_{\mathrm{X}} = 4 \times 10^{37}$ ergs s^{-1}. Given the overall uncertainties, this is in good agreement with the observed value (9.5×10^{37} ergs s^{-1}; see Table 2). In a more typical low-density environment $n_0 \simeq 0.1$ cm^{-3}, the X-ray luminosity is only on the order of $L_{\mathrm{X}} = 1 \times 10^{36}$ ergs s^{-1}, i.e., below the sensitivity of our *ROSAT* data.

What does this imply? Simply put, the vast majority of superbubbles are far too faint to have been detected by *ROSAT*. Those that have been are, in some sense, peculiar. One method to boost the X-ray luminosity, and increase the X-ray–emitting lifetime, would be to invoke mass loading (Arthur & Henney 1986). Besides, there remains the possibility that these cases are associated with X-ray binaries rather than plasma-filled superbubbles. For example, in the case of IC 2574, owing to the limited angular resolution of the *ROSAT* PSPC, it was not possible to differentiate between the X-ray emission originating from hot gas and the thermal emission from an unresolved individual X-ray source, as now seems likely on the basis of our *Chandra* data of IC 2574.

These unresolved sources do have the same luminosities, on the order of 10^{38} ergs s^{-1}, as supershells. Alternatively, there could be a contribution to a thermal plasma by supernovae developing in a dense environment, such as SN 1988Z, which reportedly reached an X-ray luminosity of 10^{41} ergs s^{-1} (Fabian & Terlevich 1996).

Moreover, it might be difficult to detect coronal gas from expanding superbubbles as there could be a conspiracy at work. Perhaps only (super)bubbles in the making, which are still actively being powered and hence overpressured, would be sufficiently bright to be seen by, for example, *ROSAT*. However, these objects tend to be fairly small, young, and surrounded by a dense H I shell that would absorb the X-rays, especially the softer ones. Once a bubble has reached its final size, after some 10^8 yr, the interior has cooled down to below 10^6 K, and no X-rays will be detected. It is only with the new generation of satellites, such as *Chandra* and *XMM-Newton*, that we can hope to settle this issue once and for all.

6. SUMMARY AND CONCLUSIONS

We analyzed *ROSAT* PSPC data of the dwarf galaxy Holmberg II. The *ROSAT* data provide information on faint X-ray emission features down to a 3 σ unabsorbed limiting flux of $F_X \simeq 4 \times 10^{-15}$ ergs cm^{-2} s^{-1}. This corresponds to a luminosity threshold of $L_X \geq 10^{37}$ergs s^{-1}. In total, we detected 31 significant X-ray sources located within the H I column density distribution of Ho II. Using the log N versus log S relation of Hasinger et al. (1998), we expect to detect about seven XRB sources within the area of Ho II H I gas disk. To avoid confusion with unrelated extragalactic XRB sources, we investigated further only those X-ray sources which have counterparts in FUV, Hα, or radio continuum emission. This additional selection criterion is fulfilled by 13 X-ray sources.

In order to determine the nature of faint X-ray sources for which no high signal-to-noise spectral information can be obtained, we applied the technique of the hardness ratio diagram. For this purpose, we evaluated the intensities in the broad *ROSAT* $\frac{1}{4}$, $\frac{3}{4}$, and 1.5 keV energy band and calculated the corresponding X-ray hardness ratios. Depending on the amount of photoelectric attenuation, an X-ray source will fall within a specific zone in this diagram. In analogy with the optical regime, one can consider the variation of the X-ray color owing to photoelectric absorption as the counterpart for reddening of stellar light by intervening dust. The X-ray hardness ratio diagram offers a very sensitive tool to constrain the X-ray–emitting process even for faint sources. The faintest source analyzed in this paper has an X-ray flux of only $F_X(0.1\text{–}2.4 \text{ keV}) = 11 \times 10^{-15}$ ergs cm^{-2} s^{-1} (source 1).

Of the 13 sources detected with confidence and for which counterparts at other wavelengths have been found, we speculate that on the order of 3 are young SNRs, three are associated with regions of active star formation, one might be the superposed contribution of the coronal X-ray emission of several hundred O stars, and on the order of 5 are most likely X-ray binaries. The strongest source, source 13, was already studied previously by Zezas et al. (1999). Whereas they claim a power-law spectrum and relatively high absorbing column density of about $N_{H\,I} = 1.2 \times 10^{21}$ cm^{-2}, and suggest some source of accretion on to a compact object, we prefer to interpret this source as having a softer intrinsic spectrum, and an absorbing column density of only $N_{H\,I} = 4 \times 10^{20}$ cm^{-2}. Our analysis leads us to propose that this source is most likely an SNR. This is supported by the analysis published by Miyaji et al. (2001), who find that some 27% of the *ROSAT* X-ray emission comes from an extended source and that the spectrum below 2.5 keV is best fitted by a thermal plasma. However, their *ASCA* observations show that above 2.5 keV this source shows a power-law spectrum that they ascribe to accretion on to an intermediate-mass black hole.

No extended emission that could be attributed to hot gas filling the H I superbubbles was detected above our *ROSAT* luminosity limit of $L_{limit}(0.1\text{–}2.1 \text{ keV}) \geq 10^{37}$ ergs s^{-1}. This is not too surprising and in agreement with theoretical estimates that predict luminosities of $L_X \approx 10^{36}\text{–}10^{37}$ ergs s^{-1}.

As mentioned, observations with *Chandra* and *XMM-Newton* will be needed and are expected to be especially rewarding for studying the ISM in nearby (dwarf) galaxies.

We wish to thank an anonymous referee for careful reading of the manuscript and a number of good comments that improved the presentation of the paper. J. K. was supported by the Deutsches Zentrum für Luft- und Raumfahrt under grant 50 OR 0103. F. W. acknowledges National Science Foundation grant AST96-13717; E. B. was supported by a research grant from CONACyT (27606-E).

REFERENCES

Arthur, S. J., & Henney, W. J. 1996, ApJ, 457, 752
Bomans, D. J., Chu, Y.-H., & Hopp, U. 1997, AJ, 113, 1678
Bomans, D. J., Dennerl, K., & Kürster, M. 1994, A&A, 283, L21
Bureau, M., & Carignan, C. 1997, in 23rd IAU Meeting, Joint Discussion 2, Dwarf Galaxies: Probes for Galaxy Formation and Evolution, ed. S. Takahira (Kyoto: IAU), 36
Chu, Y.-H., Chang, H.-W., Su, Y.-L., & Mac Low, M.-M. 1995, ApJ, 450, 157
Chu, Y.-H., & Mac Low, M.-M. 1990, ApJ, 365, 510
Chu, Y.-H., Mac Low, M.-M., Garcia-Segura, G., Wakker, B. P., & Kennicutt, R. C. 1993, ApJ, 414, 213
Egger, R. J., & Aschenbach, B. 1995, A&A, 294, L25
Fabbiano, G. 1989, ARA&A, 27, 87
———. 1996, in Röntgenstrahlung from the Universe, ed. H. U. Zimmerman, J. E. Trümper, & H. Yorke (MPE Rep. 263; Garching: MPE), 347
Fabian, A. C., & Terlevich, R. 1996, MNRAS, 280, L5
Gendreau, K. C., et al. 1995, PASJ, 47, L5
Hartmann, D., & Burton, W. B. 1997, Atlas of Galactic Neutral Hydrogen (Cambridge: Cambridge Univ. Press)
Hasinger, G., et al. 1998, A&A, 329, 482
Hunter, D. A., & Gallagher, J. S. 1985, ApJS, 58, 533
Kudritzki, R. P., Palsa, R., Feldmeier, A., Puls, J., & Pauldrach, A. W. A. 1995, in Röntgenstrahlung from the Universe, ed. H. U. Zimmerman, J. E. Trümper, & H. Yorke (MPE Rep. 263; Garching: MPE), 9
Mac Low, M.-M., Chang, T. H., Chu, Y.-H., Points, S. D., Smith, R. C., & Wakker, B. P. 1998, ApJ, 493, 260
Martin, C. L., & Kennicutt, R. C. 1995, ApJ, 447, 171
Mashchenko, S. Y., & Silich, S. A. 1995, Astron. Rep., 39, 587
Miller, B. W. 1995, ApJ, 446, L75
Miyaji, T., Lehmann, I., & Hasinger, G. 2001, AJ, 121, 3041
Mushotzky, R. F., Cowie, L. L., Barger, A. J., & Arnaud, K. A. 2000, Nature, 404, 459
Oey, M. S., & Clarke, C. J. 1997, MNRAS, 289, 570
Puche, D., Westpfahl, D., Brinks, E., & Roy, J.-R. 1992, AJ, 103, 1841
Raymond, J. C., & Smith, B. W. 1977, ApJS, 35, 419
Rhode, K. L., Salzer, J. J., Westpfahl, D. J., & Radice, L. A. 1999, AJ, 118, 323
Sfeir, D. M., Lallement, R., Crifo, F., & Welsh, B. Y. 1999, A&A, 346, 785
Silich, S. A., Tenorio-Tagle, G., Terlevich, R., Terlevich, E., & Netzer, H. 2001, MNRAS, 324, 191
Stewart, S. G., et al. 2000, ApJ, 529, 201
Sutherland, R. S., & Dopita, M. A. 1993, ApJS, 88, 253
Tongue, T. D., & Westpfahl, D. J. 1995, AJ, 109, 2462
Walter, F., & Brinks, E. 1999, AJ, 118, 273
Walter, F., Kerp, J., Duric, N., Brinks, E., & Klein, U. 1998, ApJ, 502, L143
Weaver, R., McCray, R., Castor, J., Shapiro, P., & Moore, R. 1977, ApJ, 218, 377
White, N. E., Swank, J. H., & Holt, S. S. 1983, ApJ, 270, 711
Zezas, A. L., Georgantopoulos, I., & Ward, M. J. 1999, MNRAS, 308, 302
Zimmermann, U., et al. 1998, EXSAS User Guide (MPE Rep. 257, updated; Garching: MPE)